Bound States and Field-Polarized Haldane Modes in a Quantum Spin Ladder

S. Ward,[1,2,3] M. Mena,[1,2,3] P. Bouillot,[4,5] C. Kollath,[3,6] T. Giamarchi,[3] K. P. Schmidt,[7] B. Normand,[1] K. W. Krämer,[8] D. Biner,[8] R. Bewley,[9] T. Guidi,[9] M. Boehm,[10] D. F. McMorrow,[2] and Ch. Rüegg[1,3]

[1]*Laboratory for Neutron Scattering and Imaging, Paul Scherrer Institut, CH-5232 Villigen PSI, Switzerland*
[2]*London Centre for Nanotechnology and Department of Physics and Astronomy, University College London, London WC1E 6BT, United Kingdom*
[3]*Department of Quantum Matter Physics, University of Geneva, CH-1211 Geneva, Switzerland*
[4]*Department of Medical Imaging and Information Sciences, Interventional Neuroradiology Unit, University Hospitals of Geneva, CH-1211 Geneva, Switzerland*
[5]*Laboratory for Hydraulic Machines, École Polytechnique Fédérale de Lausanne, CH-1015 Lausanne, Switzerland*
[6]*HISKP, University of Bonn, Nussallee 14-16, 53115 Bonn, Germany*
[7]*Theoretische Physik I, Staudtstrasse 7, FAU Erlangen-Nürnberg, 91058 Erlangen, Germany*
[8]*Department of Chemistry and Biochemistry, University of Bern, CH-3012 Bern, Switzerland*
[9]*ISIS Facility, Rutherford Appleton Laboratory, Chilton, Didcot, Oxford OX11 0QX, United Kingdom*
[10]*Institut Laue Langevin, 6 rue Jules Horowitz BP156, 38024 Grenoble CEDEX 9, France*

(Received 19 August 2016; published 28 April 2017)

The challenge of one-dimensional systems is to understand their physics beyond the level of known elementary excitations. By high-resolution neutron spectroscopy in a quantum spin-ladder material, we probe the leading multiparticle excitation by characterizing the two-magnon bound state at zero field. By applying high magnetic fields, we create and select the singlet (longitudinal) and triplet (transverse) excitations of the fully spin-polarized ladder, which have not been observed previously and are close analogs of the modes anticipated in a polarized Haldane chain. Theoretical modeling of the dynamical response demonstrates our complete quantitative understanding of these states.

DOI: 10.1103/PhysRevLett.118.177202

Throughout physics, one-dimensional (1D) systems show a range of intriguing and unconventional phenomena. The dominance of quantum fluctuations in 1D materials makes them the ultimate form of quantum matter. The physics of the ground states and elementary, low-energy excitations of 1D systems are by now rather well understood in theory [1] and have been realized in experiment in a number of quite different fields, including conducting wires [2], atomic chains [3], quantum magnets [4], and ultracold atoms [5]. Looking forward, the next frontier is to understand and control the physics of these systems on all energy scales, including their multiparticle excitations and topological states.

Quantum magnets provide an excellent arena not only for quantitative measurements of the strongly correlated quantum wave function but also for its systematic control by applied external parameters [6–8]. Among the systems whose elementary magnetic excitations are already well characterized, one key model is the $S = 1/2$ "ladder," consisting of two coupled spin chains [9], with detailed experimental studies performed on genuine ladder materials including $La_4Sr_{10}Cu_{24}O_{41}$ [10], $(C_5H_{12}N)_2CuBr_4$ (BPCB) [11–17], and $(C_7H_{10}N)_2CuBr_4$ (DIMPY) [18–21]. The ladder has many parallels to another cornerstone model, the Haldane ($S = 1$) chain [22,23], and significant progress has been made in calculating the dynamical response of both systems [24]. However, genuine Haldane materials with accessible energy scales have proven difficult to find [25–27], and thus the response in strong magnetic fields remains an open problem [28,29].

In this Letter, we report on measurements of single- and multimagnon excitations in the spin ladder bis-piperidinium copper tetrachloride (BPCC). By exploiting the elegant parity selectivity of the ladder geometry, at zero field we demonstrate the presence of a strong two-magnon bound-state triplet over half of the Brillouin zone and quantify its spectral weight. At high fields, we demonstrate the selection criteria for the singlet excitation, or amplitude mode, of the fully field-polarized (FP) phase, as well as for its triplet (transverse) mode. Both are unknown in a conventional ferromagnet and have direct analogs in the FP Haldane chain. By detailed analytical and numerical modeling, we describe our intensity measurements with quantitative accuracy.

The spin ladder has two basic magnetic interactions, the rung (J_r) and leg (J_l) couplings, and one ratio, $\gamma = J_l/J_r$. BPCB ($\gamma \simeq 0.26$) and DIMPY ($\gamma \simeq 1.7$) exemplify contrasting regimes of ladder behavior. The deuterated chloride analog of BPCB, $(C_5D_{12}N)_2CuCl_4$ (BPCC) crystallizes in the same monoclinic space group, $P2_1/c$, shown in Fig. S1 of the Supplemental Material (SM) [30]. Two halide bridges between pairs of Cu^{2+} ions form the rung dimer (J_r). A further halide bridge between ions repeating periodically in $\hat{a}$ provides J_l. BPCC is an exceptional realization of a very clean $S = 1/2$ spin ladder with three

attributes ideal for our studies. First, the ladders are well separated by piperidinium groups, making them effectively isolated, as shown in Sec. S2 of the SM [30]. Second, the ratio $\gamma \simeq 0.4$ [41] is perfectly suited for observing bound states in the two-magnon sector (whose weight scales with γ^2), without strong interference from scattering states. Third, the low energy scales in BPCC [41,42] allow one to work well within the FP phase at laboratory magnetic fields.

High-quality deuterated single-crystal samples were synthesized and five crystals of total mass 2.4 g were coaligned on the MORPHEUS instrument at SINQ for the collection of inelastic neutron scattering data on the time-of-flight spectrometer LET at ISIS [43]. The sample was mounted inside a 9 T vertical cryomagnet, on a dilution insert with a stable base temperature of 60 mK. Frame-rate multiplication was used with a primary incoming neutron energy of 2.5 meV. Data at zero field were collected at 104 sample rotation angles and processed using the MANTID program [44]. The resulting data sets for the dynamical structure factor, $S(\mathbf{Q},\omega)$, were analyzed with the HORACE software package [45].

In the two-leg ladder, the rung-singlet wave function is antisymmetric whereas the triplets are symmetric, as represented schematically in Figs. 1(g) and 1(i). This geometry therefore allows a full parity selection between odd ($q_y = \pi$, e.g., singlet-triplet) and even ($q_y = 0$, e.g. triplet-triplet) excitation processes [24,46], where q_y is the wave vector across the ladder unit. There is no mixing between modes of opposite parity and $S(\mathbf{Q},\omega)$ separates completely into odd- and even-parity sectors, whose intensity maxima occur in very different parts of the Brillouin zone, as shown in Fig. S2 of the SM [30]. Although the crystallography of BPCC dictates that there are two different ladder orientations (Fig. S1 of the SM [30]), this parity selection remains possible [24,46] (Sec. S1 of the SM [30]).

We begin our presentation at zero applied field. We refer to the elementary one-triplet excitation of the ladder as a "magnon." The one-magnon dispersion relation, $\omega(q)$, is clearly evident in Fig. 1(a), where the 4D intensity data set is analyzed to select the $q_y = \pi$ sector. Our data treatment is discussed in Sec. S2 of the SM [30]. We observe an excitation with gap 0.2 meV, bandwidth 0.23 meV, and periodicity 2π, suggesting that J_r is significantly stronger than J_l.

Several theoretical approaches give good descriptions of the two-leg ladder in the strong-rung regime. From an optimized fit of the one-magnon data to a third-order strong-coupling expansion [47] [Eq. (S5) of Sec. S3 of the SM [30]], we deduce the exchange parameters $J_r = 0.295(8)$ meV and $J_l = 0.116(1)$ meV; the resulting dispersion is shown as the red lines in Figs. 1(a) and 1(c). The corresponding values from the bond-operator technique [48] [Eq. (S6) of the SM [30]] are $J_r = 0.306(8)$ meV and $J_l = 0.113(1)$ meV, and the dispersion is identical within the error bars. Thus, the leg exchange in BPCC, with $\gamma \simeq 0.39$, is more significant than in BPCB, which is the

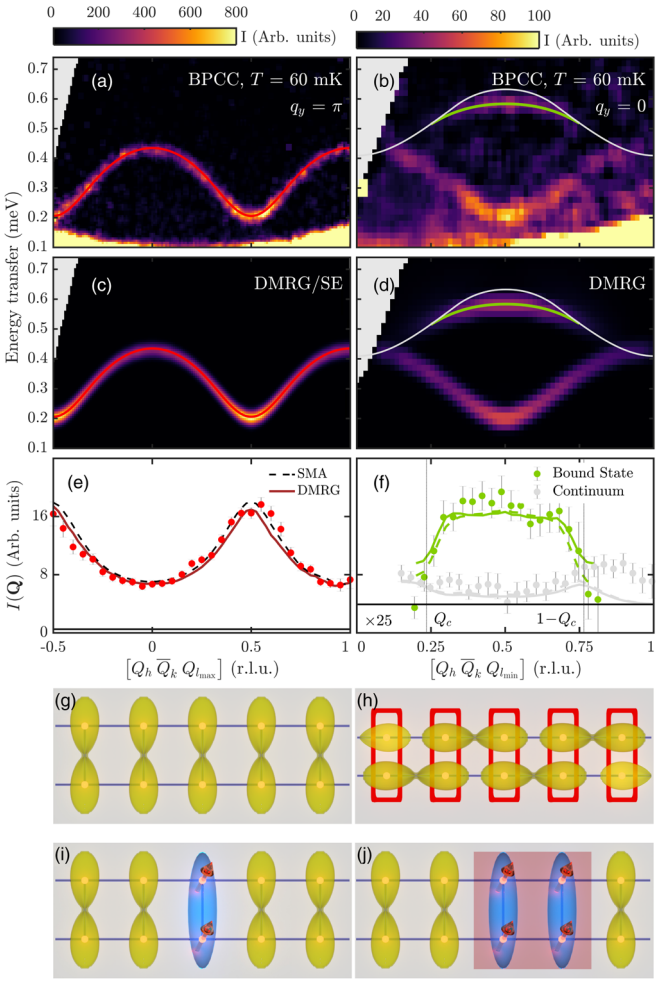

FIG. 1. One- and two-magnon excitations in BPCC. (a) $S(\mathbf{Q},\omega)$ measured in the $q_y = \pi$ sector. The solid red line is the dispersion obtained from strong-coupling [Eq. (S5) of the SM [30]] and bond-operator treatments [Eq. (S6) of the SM [30]]. (b) $S(\mathbf{Q},\omega)$ measured for $q_y = 0$. The green line indicates the dispersion [Eq. (S8) of the SM [30]] and range [Eq. (1)] over which the triplet component of the two-magnon bound state is expected in BPCC. The white line marks the boundary of the two-magnon continuum [Eq. (S9) of the SM [30]]. (c) $S(\mathbf{Q},\omega)$ for $q_y = \pi$ obtained by DMRG and SE calculations, whose results are indistinguishable. (d) $S(\mathbf{Q},\omega)$ from DMRG for $q_y = 0$. (e) $I(\mathbf{Q})$ obtained by integration over Q_k (denoted $\bar{Q}_k$) and over the energy range $0.19 \le \omega \le 0.43$ meV, shown as red points and computed in the SMA (dashed black) and by DMRG (solid red lines); the solid black line denotes the background and $Q_{l_{max}}$ is defined in Eq. (S4) of the SM [30]. (f) Bound-state (green) and continuum (gray) contributions to $I(\mathbf{Q})$, obtained by integrating over energy windows below and above the two-magnon continuum edge; measured intensities (points) are compared with DMRG (solid line) and SE (dashed line) calculations. The black line denotes the background and $Q_{l_{min}}$ is defined in Eq. (S4) of the SM [30]. (g) Ground state of antisymmetric rung singlets in the two-leg ladder. (h) Ground state of the Haldane chain in the representation of auxiliary $S = 1/2$ spin pairs; red boxes represent the operator projecting the two spins at each site to a real $S = 1$ state. (i) One-magnon excited state, a single symmetric rung triplet. (j) Two-magnon excited state, a triplet pair.

key to our quantitative observations of bound states. We perform both density-matrix renormalization-group (DMRG) and systematic high-order series-expansion (SE) calculations for $S(\mathbf{Q},\omega)$ (Sec. S3 of the SM [30]), which capture the contributions of all excitation channels; with optimized parameters $J_r = 0.295(0.294)$ meV and $J_l = 0.115(0.117)$ meV for DMRG (SE), both yield excellent agreement with the one-magnon measurements, as shown in Fig. 1(c). These slightly differing parameter values converge as expected with the increasing sophistication (decreasing bias) of the theoretical approach, namely bond-operator, SE with increasing expansion orders, DMRG.

For a quantitative discussion of the scattering intensity, we integrate $S(\mathbf{Q},\omega)$ over specific energy ranges and consider the resulting structure factor, $I(\mathbf{Q})$. The quantity $I(\mathbf{Q})$ obtained by integrating over the full one-magnon energy range ($0.19 \leq \omega \leq 0.43$ meV) is shown in Fig. 1(e). Our DMRG (solid line) and SE calculations reproduce not only the dispersion but also the spectral weight to very high accuracy. To analyze the one-magnon intensity, we exploit the dominance of this mode in the spectrum to apply the single-mode approximation (SMA) (Sec. S3 of the SM [30]). With prior knowledge of J_r and J_l, the average spin correlations, $\langle \mathbf{S}_1 \cdot \mathbf{S}_2 \rangle$, can be extracted separately for the rung and leg bonds [48]. Here, however, the unknown overall scale factor restricts us to deducing their ratio [46], whose expected theoretical value is 0.26(1). From our data, we obtain a correlation ratio of 0.22(1) and the fit to $I(\mathbf{Q})$ shown by the dashed line in Fig. 1(e). Thus, our one-magnon intensity measurements both quantify the correlations, and, hence, the entanglement, in the quantum wave function (Sec. S3 of the SM [30]) and set the scale factor for intensity calculations in all other scattering sectors.

Next we consider multimagnon excitations. The symmetric ($q_y = 0$) channel is the maximum of all processes changing the triplet count by an even number and is dominated by two-magnon excitations. We exploit the parity of the ladder structure to separate their intensity contributions unambiguously (Sec. S1 of the SM [30]) and we show $S(\mathbf{Q},\omega)$ in Fig. 1(b). Two magnons whose wave vectors, k and $q-k$, are in low-lying parts of the one-magnon band may form a bound state, a dispersive quasiparticle whose energy, $\omega_B(q)$, lies below all possible states of two unbound magnons $[\omega(k)+\omega(q-k)]$ [49,50], which form a scattering continuum. The zero-field spectrum of DIMPY has been found to exhibit both bound and continuum features [20]. However, in BPCC the continuum contributions are extremely weak, allowing the dispersion, spectral weight, and termination of the two-magnon bound state to be measured in a degree of detail extremely difficult to achieve either in DIMPY or in the dimerized-chain material $Cu(NO_3)_2 \cdot 2.5D_2O$ [51].

In Fig. 1(b) we observe a clear, discrete mode lying at an energy of 0.58 meV at $Q_h = 0.5$, below the continuum edge, and dispersing downwards before disappearing into the continuum, whose contribution is indiscernible. From the selection rules for neutron scattering, this mode is the triplet branch ($S_{\mathrm{tot}} = 1$) of the two-magnon bound state. The singlet ($S_{\mathrm{tot}} = 0$) branch is detectable by light scattering [52], and both singlet and quintet ($S_{\mathrm{tot}} = 2$) branches by neutron spectroscopy at higher temperatures [53]. We note that one-magnon spectral weight is detectable in this sector because the geometry of BPCC excludes perfect destructive interference (Sec. S1 of the SM [30]). However, in contrast to the discussion of magnon "termination" [54], here the one- and two-magnon excitations are prevented by their opposite parities from mixing where they overlap in energy [as can be seen in Figs. 1(a) and 1(b)]. The primary characteristics of both types of excitation are summarized in the left-hand columns of Table I.

The bound state overlaps with the two-magnon continuum below a critical wave vector, Q_c, and decays very readily in this range [55]. It is therefore clearly visible only when $Q_c < Q_h < 1 - Q_c$, with

$$Q_c = \frac{1}{3} - \frac{5}{4\sqrt{3}\pi}\gamma - \frac{109}{96\sqrt{3}\pi}\gamma^2 + \mathcal{O}(\gamma^3), \qquad (1)$$

in a strong-coupling expansion (Sec. S3 of the SM [30]). For BPCC, Eq. (1) with $\gamma = 0.39$ leads to $Q_c = 0.212$. However, this value of γ lies well in the regime where high orders are required for an accurate description. A range of $0.235 \leq Q_h \leq 0.765$ is computed in Ref. [55] by working to 12th order in γ, and in Fig. 1(d) we require the tenth-order dispersion of the two-magnon bound state [56] and the continuum edge. From our DMRG and SE calculations, we find that both the dispersion [Fig. 1(d) and Figs. S3(a) and S3(c) of the SM [30]] and the scattered intensity [Fig. 1(f) and Figs. S3(b) and S3(d) of the SM [30]] agree exceptionally well with the data. Thus, our results also

TABLE I. Summary of characteristics of the spin excitations measured in the two-leg ladder at zero field (left-hand columns) and in the FP regime (right). s, symmetric; a, antisymmetric; l, longitudinal; t, transverse. n is the number of excited magnons, S_{tot} the total spin, and S_z the spin component along the z axis, which corresponds to the applied field direction. N represents the total number of sites in the ladder. Italic quantum numbers for the two-magnon excitation indicate physical processes not observable by neutron scattering.

	$H = 0$		$H > H_s$	
Parity	$q_y = \pi$	$q_y = 0$	$q_y = \pi$	$q_y = 0$
Symmetry	a	s	a	s
Polarization			l	t
n	1	2	-1	0
S_{tot}	$0 \to 1$	$0 \to 0, 1, 2$	$\frac{N}{2} \to \frac{N}{2}-1$	$\frac{N}{2} \to \frac{N}{2}$
ΔS_{tot}	1	$0, 1, 2$	-1	0
S_z	$0 \to 0, \pm 1$	$0 \to 0, \pm 1, \pm 2$	$\frac{N}{2} \to \frac{N}{2}-1$	$\frac{N}{2} \to \frac{N}{2}-1$
ΔS_z	$0, \pm 1$	$0, \pm 1, \pm 2$	-1	-1

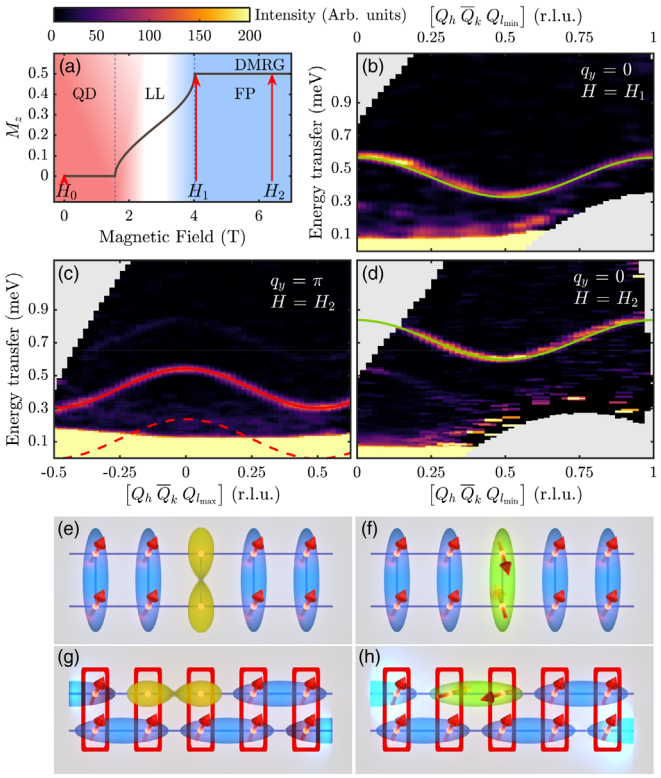

FIG. 2. Excitations in fully polarized BPCC. (a) Magnetization of BPCC (from DMRG) superimposed on the field-induced phase diagram; LL denotes the Luttinger-liquid and QD the quantum disordered phase. (b) $S(\mathbf{Q},\omega)$ measured at $H_1 = 4.067$ T $\simeq H_s$ and (d) $H_2 = 6.141$ T, both in the $q_y = 0$ sector. (c) $S(\mathbf{Q},\omega)$ measured at H_2 in the $q_y = \pi$ sector. Green and red solid lines are, respectively, fits to the triplet ($q_y = 0$) and singlet ($q_y = \pi$) modes using Eq. (2). The dashed line in panel (c) indicates the position of the singlet at H_s (not measured due to dominant nuclear incoherent scattering at low energies). (e) Schematic representation of a FP two-leg ladder with one rung-singlet excitation. (f) FP ladder with one rung-triplet (t_0) excitation. (g) FP Haldane chain in the auxiliary-spin representation containing one leg-singlet and (h) one leg-triplet excitation.

quantify the termination of the bound state [Fig. 1(f) and Sec. S3 of the SM [30]].

We turn now to the excitation spectrum at high magnetic fields. Quantum magnets with low exchange energies exhibit field-induced critical points marking transitions between several types of exotic quantum phase in materials including Cs_2CuCl_4 [57], $CuSO_4 \cdot 5D_2O$ [58], and BPCB [13,14,16]. For two-leg ladders, the physics of the intermediate-field, "Luttinger-liquid" (LL) regime [Fig. 2(a)], which possesses a continuum of gapless, fractional spin excitations, has been studied in depth in BPCB, and we do not repeat this analysis for BPCC here.

However, in all ladder materials studied to date, the dynamical properties have been measured only below (DIMPY, $H_s \simeq 29$ T [20,21]) or at the saturation field (BPCB, $H_s = 14$ T [16]). The exchange parameters of BPCC place full saturation well within our instrumental capabilities. Here we present previously unavailable measurements of the spectrum of the FP ladder.

Figure 2 shows the dynamical structure factor of FP BPCC. Parity remains a good quantum number at high fields, and in each sector we find one mode. At $H_s \simeq H_1 = 4.067$ T, in the $q_y = 0$ sector we observe [Fig. 2(b)] a mode with a purely sinusoidal dispersion and a gap of 0.3 meV (J_r). On increasing the field to $H_2 = 6.141$ T [Fig. 2(d)], this gap increases linearly with H. At H_2 with $q_y = \pi$, we observe a mode with identical dispersion but a gap smaller by precisely J_r [Fig. 2(c)].

The FP ground state is one of "up-up" triplets, $|t_+\rangle = |\uparrow\uparrow\rangle$, on every ladder rung. Parity selection separates triplet-singlet ($q_y = \pi$) from triplet-triplet excitations ($q_y = 0$). The excitations of the FP phase are quite unlike the modes of a ferromagnet, with or without an applied field, not least in that the band minimum remains at $q_h = \pi$. Although all FP excitations are $\Delta S_z = -1$, this can be achieved with $\Delta S_{\rm tot} = 0$ or $\Delta S_{\rm tot} = -1$. The ladder provides a transparent situation where the latter is simply the singlet excitation of a rung [Fig. 2(e)] and the former the t_0 triplet [Fig. 2(f)]. The nature and quantum numbers of these modes are summarized in the right-hand columns of Table I.

The bond-operator method is exact at $H \geq H_s$, where quantum fluctuations are completely quenched, giving the excitations (Sec. S3 of the SM [30])

$$\omega_s(q) = g\mu_B(H - H_s) + J_l(1 + \cos q),$$
$$\omega_0(q) = g\mu_B(H - H_s) + J_r + J_l(1 + \cos q), \qquad (2)$$

with $H_s = (J_r + 2J_l)/g\mu_B$. The upper triplet mode, t_-, is invisible to neutron scattering and has no dispersion. The singlet branch is a longitudinal, or amplitude, mode of the field-enforced order, and is gapless at H_s but has a gap of $H - H_s$ above this field; being antisymmetric, it is found with $q_y = \pi$, as in Fig. 2(c). The $\Delta S_{\rm tot} = 0$ excitation is the gapped triplet, t_0, a transverse spin mode, which by its symmetric nature is observed in Figs. 2(b) and 2(d), lying higher than the singlet by energy J_r [Eq. (2)]. By simultaneous fits to Eq. (2) at H_1 and H_2, we find that exchange parameters $J_r = 0.294(1)$ meV and $J_l = 0.120(1)$ meV, combined with a g value of 2.26(1), provide an extremely accurate account of the data.

We comment that excitations directly analogous to the singlet and t_0 triplet should also be expected in the $S = 1$ chain at $H > H_s$. The mathematical Affleck-Kennedy-Lieb-Tasaki (AKLT) description [23] of the Haldane chain in terms of leg singlets formed from auxiliary $S = 1/2$ spins, depicted in Fig. 1(h), was famously demonstrated to have real experimental meaning [59,60]. Figures 2(g) and 2(h) represent the singlet and t_0 excitation of leg triplets formed from these $S = 1/2$ entities in the FP Haldane chain. While the lowest (singlet) mode has been measured

in FP BPCB [16], the t_0 mode has not been observed in any other ladder or Haldane system; it is also expected in FP alternating-chain materials, such as $Cu(NO_3)_2 \cdot 2.5D_2O$ [61], although its interpretation is more complicated in the absence of parity selection.

In summary, we have measured the magnetic excitations of the two-leg ladder BPCC at all wave vectors and magnetic fields. At zero field, we exploit the parity selectivity of the ladder to achieve a total separation of the one- and two-triplet excitation sectors, finding the clearest known example of the two-magnon bound state. In the fully spin-polarized regime, we select the gapped singlet (amplitude) and triplet (phase) modes of the ladder. Thus, we provide a systematic understanding of the magnetic excitations in a broad family of gapped 1D quantum magnets, including ladder, alternating-chain, and Haldane systems. For BPCC, we demonstrate that the magnetic response can be modeled with complete quantitative accuracy, in both dispersion and intensity, by modern DMRG and series-expansion techniques.

This work was supported by the Swiss National Science Foundation, the ERC Grant Hyper Quantum Criticality (HyperQC), the German Research Society (DFG), the EPSRC, and the UK Royal Society. It is based on experiments performed at the Swiss Spallation Neutron Source SINQ at the Paul Scherrer Institute and at the UK spallation neutron source ISIS at the Rutherford-Appleton Laboratory.

[1] T. Giamarchi, *Quantum Physics in One Dimension* (Oxford University Press, New York, 2004).
[2] O. M. Auslaender, H. Steinberg, A. Yacoby, Y. Tserkovnyak, B. I. Halperin, K. W. Baldwin, L. N. Pfeiffer, and K. W. West, Science **308**, 88 (2005).
[3] S. Nadj-Perge, I. K. Drozdov, J. Li, H. Chen, S. Jeon, J. Seo1, A. H. MacDonald, B. A. Bernevig, and A. Yazdani, Science **346**, 602 (2014).
[4] H.-J. Mikeska and A. K. Kolezhuk, Lect. Notes Phys. **645**, 1 (2004).
[5] M. A. Cazalilla, R. Citro, T. Giamarchi, E. Orignac, and M. Rigol, Rev. Mod. Phys. **83**, 1405 (2011); X.-W. Guan, M. T. Batchelor, and C. Lee, Rev. Mod. Phys. **85**, 1633 (2013).
[6] See T. Giamarchi, Ch. Rüegg, and O. Tchernyshyov, Nat. Phys. **4**, 198 (2008), and references therein.
[7] S. Ward, P. Bouillot, H. Ryll, K. Kiefer, K. W. Krämer, Ch. Rüegg, C. Kollath, and T. Giamarchi, J. Phys. Condens. Matter **25**, 014004 (2013).
[8] P. Merchant, B. Normand, K. W. Krämer, M. Boehm, D. F. McMorrow, and Ch. Rüegg, Nat. Phys. **10**, 373 (2014).
[9] See E. Dagotto and T. M. Rice, Science **271**, 618 (1996), and references therein.
[10] S. Notbohm, P. Ribeiro, B. Lake, D. A. Tennant, K. P. Schmidt, G. S. Uhrig, C. Hess, R. Klingeler, G. Behr, B. Büchner, M. Reehuis, R. I. Bewley, C. D. Frost, P. Manuel, and R. S. Eccleston, Phys. Rev. Lett. **98**, 027403 (2007).
[11] B. R. Patyal, B. L. Scott, and R. D. Willett, Phys. Rev. B **41**, 1657 (1990).
[12] B. C. Watson, V. N. Kotov, M. W. Meisel, D. W. Hall, G. E. Granroth, W. T. Montfrooij, S. E. Nagler, D. A. Jensen, R. Backov, M. A. Petruska, G. E. Fanucci, and D. R. Talham, Phys. Rev. Lett. **86**, 5168 (2001).
[13] Ch. Rüegg, K. Kiefer, B. Thielemann, D. F. McMorrow, V. Zapf, B. Normand, M. B. Zvonarev, P. Bouillot, C. Kollath, T. Giamarchi, S. Capponi, D. Poilblanc, D. Biner, and K. W. Krämer, Phys. Rev. Lett. **101**, 247202 (2008).
[14] M. Klanjšek, H. Mayaffre, C. Berthier, M. Horvatić, B. Chiari, O. Piovesana, P. Bouillot, C. Kollath, E. Orignac, R. Citro, and T. Giamarchi, Phys. Rev. Lett. **101**, 137207 (2008).
[15] T. Lorenz, O. Heyer, M. Garst, F. Anfuso, A. Rosch, Ch. Rüegg, and K. Krämer, Phys. Rev. Lett. **100**, 067208 (2008); F. Anfuso, M. Garst, A. Rosch, O. Heyer, T. Lorenz, Ch. Rüegg, and K. Krämer, Phys. Rev. B **77**, 235113 (2008).
[16] B. Thielemann, C. Rüegg, H. M. Rønnow, A. M. Läuchli, J. S. Caux, B. Normand, D. Biner, K. W. Krämer, H. U. Güdel, J. Stahn, K. Habicht, K. Kiefer, M. Boehm, D. F. McMorrow, and J. Mesot, Phys. Rev. Lett. **102**, 107204 (2009).
[17] B. Thielemann *et al.*, Phys. Rev. B **79**, 020408(R) (2009).
[18] A. Shapiro, C. P. Landee, M. M. Turnbull, J. Jornet, M. Deumal, J. J. Novoa, M. A. Robb, and W. Lewis, J. Am. Chem. Soc. **129**, 952 (2007).
[19] T. Hong, Y. H. Kim, C. Hotta, Y. Takano, G. Tremelling, M. M. Turnbull, C. P. Landee, H.-J. Kang, N. B. Christensen, K. Lefmann, K. P. Schmidt, G. S. Uhrig, and C. Broholm, Phys. Rev. Lett. **105**, 137207 (2010).
[20] D. Schmidiger, P. Bouillot, S. Mühlbauer, S. Gvasaliya, C. Kollath, T. Giamarchi, and A. Zheludev, Phys. Rev. Lett. **108**, 167201 (2012); D. Schmidiger, S. Mühlbauer, A. Zheludev, P. Bouillot, T. Giamarchi, C. Kollath, G. Ehlers, and A. M. Tsvelik, Phys. Rev. B **88**, 094411 (2013).
[21] D. Schmidiger, P. Bouillot, T. Guidi, R. Bewley, C. Kollath, T. Giamarchi, and A. Zheludev, Phys. Rev. Lett. **111**, 107202 (2013).
[22] F. D. M. Haldane, Phys. Rev. Lett. **50**, 1153 (1983); Phys. Lett. **93A**, 464 (1983).
[23] I. Affleck, T. Kennedy, E. H. Lieb, and H. Tasaki, Phys. Rev. Lett. **59**, 799 (1987); Commun. Math. Phys. **115**, 477 (1988).
[24] P. Bouillot, C. Kollath, A. M. Läuchli, M. Zvonarev, B. Thielemann, C. Rüegg, E. Orignac, R. Citro, M. Klanjšek, C. Berthier, M. Horvatić, and T. Giamarchi, Phys. Rev. B **83**, 054407 (2011).
[25] A. Zheludev, Z. Honda, C. L. Broholm, K. Katsumata, S. M. Shapiro, A. Kolezhuk, S. Park, and Y. Qiu, Phys. Rev. B **68**, 134438 (2003).
[26] A. K. Bera, B. Lake, A. T. M. N. Islam, and A. Schneidewind, Phys. Rev. B **92**, 060412(R) (2015).
[27] V. S. Zapf, D. Zocco, B. R. Hansen, M. Jaime, N. Harrison, C. D. Batista, M. Kenzelmann, C. Niedermayer, A. Lacerda, and A. Paduan-Filho, Phys. Rev. Lett. **96**, 077204 (2006).
[28] A. K. Kolezhuk and H.-J. Mikeska, Prog. Theor. Phys. Suppl. **145**, 85 (2002).
[29] F. H. L. Essler and I. Affleck, J. Stat. Mech. (2004) P12006.
[30] See Supplemental Material at http://link.aps.org/supplemental/10.1103/PhysRevLett.118.177202, which includes Refs. [31–40], for details.

[31] S. Ward, S. Furuya, D. Biner, K. W. Krämer, D. Cheptiakov, M. Boehm, D. F. McMorrow, T. Giamarchi, and Ch. Rüegg (unpublished).
[32] G. Xu, C. Broholm, D. H. Reich, and M. A. Adams, Phys. Rev. Lett. **84**, 4465 (2000).
[33] B. Bauer *et al.*, J. Stat. Mech. (2011) P05001.
[34] G. Vidal, Phys. Rev. Lett. **93**, 040502 (2004).
[35] S. R. White and A. E. Feiguin, Phys. Rev. Lett. **93**, 076401 (2004).
[36] A. J. Daley, C. Kollath, U. Schollwöck, and G. Vidal, J. Stat. Mech. (2004) P04005.
[37] U. Schollwöck, Ann. Phys. (Amsterdam) **326**, 96 (2011).
[38] P. Bouillot, Ph.D. thesis, University of Geneva, 2011.
[39] C. Knetter, K. P. Schmidt, M. Grüninger, and G. S. Uhrig, Phys. Rev. Lett. **87**, 167204 (2001).
[40] C. Knetter and G. S. Uhrig, Eur. Phys. J. B **13**, 209 (2000).
[41] H. Ryll, K. Kiefer, C. Rüegg, S. Ward, K. W. Krämer, D. Biner, P. Bouillot, E. Coira, T. Giamarchi, and C. Kollath, Phys. Rev. B **89**, 144416 (2014).
[42] T. Tajiri, H. Deguchi, M. Mito, S. Takagi, H. Nojiri, T. Kawae, and K. Takeda, J. Magn. Magn. Mater. **272-276**, 1070 (2004).
[43] R. I. Bewley, J. W. Taylor, and S. M. Bennington, Nucl. Instrum. Methods Phys. Res., Sect. A **637**, 128 (2011).
[44] Available at http://www.mantidproject.org.
[45] R. A. Ewings, A. Buts, M. D. Le, J. van Duijn, I. Bustinduy, and T. G. Perring, Nucl. Instrum. Methods Phys. Res., Sect. A **834**, 132 (2016).
[46] B. Thielemann, Ph.D. thesis, ETH Zurich, 2009.
[47] M. Reigrotzki, H. Tsunetsugu, and T. M. Rice, J. Phys. Condens. Matter **6**, 9235 (1994).
[48] B. Normand and Ch. Rüegg, Phys. Rev. B **83**, 054415 (2011), and references therein.
[49] G. S. Uhrig and H. J. Schulz, Phys. Rev. B **54**, R9624 (1996); **58**, 2900(E) (1998).
[50] G. Bouzerar, A. P. Kampf, and G. I. Japaridze, Phys. Rev. B **58**, 3117 (1998).
[51] D. A. Tennant, C. Broholm, D. H. Reich, S. E. Nagler, G. E. Granroth, T. Barnes, K. Damle, G. Xu, Y. Chen, and B. C. Sales, Phys. Rev. B **67**, 054414 (2003).
[52] M. Windt, M. Grüninger, T. Nunner, C. Knetter, K. P. Schmidt, G. S. Uhrig, T. Kopp, A. Freimuth, U. Ammerahl, B. Büchner, and A. Revcolevschi, Phys. Rev. Lett. **87**, 127002 (2001).
[53] A. Honecker, F. Mila, and B. Normand, Phys. Rev. B **94**, 094402 (2016).
[54] M. B. Stone, I. A. Zaliznyak, T. Hong, C. L. Broholm, and D. H. Reich, Nature (London) **440**, 187 (2006).
[55] W. Zheng, C. J. Hamer, R. R. P. Singh, S. Trebst, and H. Monien, Phys. Rev. B **63**, 144410 (2001).
[56] C. Knetter, K. P. Schmidt, and G. S. Uhrig, Eur. Phys. J. B **36**, 525 (2003).
[57] R. Coldea, D. A. Tennant, K. Habicht, P. Smeibidl, C. Wolters, and Z. Tylczynski, Phys. Rev. Lett. **88**, 137203 (2002).
[58] M. Mourigal, M. Enderle, A. Klöpperpieper, J.-S. Caux, A. Stunault, and H. M. Rønnow, Nat. Phys. **9**, 435 (2013).
[59] M. Hagiwara, K. Katsumata, I. Affleck, B. I. Halperin, and J. P. Renard, Phys. Rev. Lett. **65**, 3181 (1990).
[60] S. H. Glarum, S. Geschwind, K. M. Lee, M. L. Kaplan, and J. Michel, Phys. Rev. Lett. **67**, 1614 (1991).
[61] M. B. Stone, Y. Chen, D. H. Reich, C. Broholm, G. Xu, J. R. D. Copley, and J. C. Cook, Phys. Rev. B **90**, 094419 (2014).